

1 Upper Ocean Response on the Passage of Tropical Cyclones in 2 the Azores Region

3 Miguel M. Lima¹, Célia M. Gouveia^{1,2}, Ricardo M. Trigo^{1,3}

4 *Correspondence to:* Miguel M. Lima

5 ¹Instituto Dom Luiz (IDL), Faculdade de Ciências, Universidade de Lisboa, 1749-016, Lisboa, Portugal

6 ²Instituto Português do Mar e da Atmosfera (IPMA), I.P., 1749-077, Rua C do Aeroporto, Lisboa, Portugal

7 ³Departamento de Meteorologia, Universidade Federal do Rio de Janeiro, Rio de Janeiro 21941-919, Brasil

8 **Abstract.** Tropical Cyclones (TCs) are extreme climate events that are known to strongly interact with the ocean
9 through two mechanisms: dynamically through the associated intense wind stress, and thermodynamically through
10 moist enthalpy exchanges at the ocean surface. These interactions contribute to relevant oceanic responses during and
11 after the passage of a TC, namely the induction of a cold wake and the production of chlorophyll (Chl-a) blooms. This
12 study aimed to understand these interactions in the Azores region, an area with relatively low cyclonic activity for the
13 North Atlantic basin, since the area experiences much less intense events than the rest of the basin. Results for the
14 1998-2020 period showed that the averaged induced anomalies were on the order of $+0.050 \text{ mg m}^{-3}$ for the Chl-a and
15 $-1.615 \text{ }^\circ\text{C}$ for SST. Furthermore, looking at the role played by several TCs characteristics we found that the intensity
16 of the TCs was the most important condition for the development of upper ocean responses. Additionally, it was found
17 that bigger TCs caused greater induced anomalies in both variables, while faster ones created greater Chl-a responses,
18 and TCs that occurred later in the season had greater TC-related anomalies. Two case studies (Ophelia, in 2017, and
19 Nadine, in 2012) were conducted to better understand each upper ocean response. Ophelia showed to affect the SST
20 at an earlier stage while the biggest Chl-a induced anomalies were registered at a later stage, allowing the conclusion
21 that thermodynamic exchanges conditioned the SST more while dynamical mixing might have played a more
22 important role in the later stage. Nadine showed the importance of the TC track geometry, revealing that the TC track
23 observed in each event can impact a specific region for longer, and therefore greater induced anomalies.

24 **Introduction**

25 Tropical Cyclones (TCs) are potentially intense atmospheric disturbances which are characterised by a low-pressure
26 centre (eye) where strong winds curl around. Among other important properties, TCs are thermodynamic dependent
27 phenomena, meaning that intense temperature gradients need to occur in the lower atmosphere to maintain and
28 intensify the storm. Thus, TCs are fed from warm sea water which provide a strong moist enthalpy flux from the
29 oceanic surface to maintain a steep temperature gradient within the lower and middle troposphere and produce massive
30 water vapour convection (Emanuel, 2003; Holton and Hakim, 2012; Pearce, 1987).

31 The strong wind stress present near the surface and the associated intense curl are also shown to induce vertical mixing
32 and Ekman upwelling in the upper layer of the ocean. In his seminal study, Price (1981) shows, through both observed
33 and numerical modelling data, the evolution of sea surface temperature (SST) on the passage of a hurricane, with the
34 emergence of a cold wake of SST after a TC due to entrainment of water from deeper layers. This effect has since
35 been well studied and documented with many case studies observed, for example, the case of Hurricane Felix, in the
36 vicinity of Bermuda in 1995, that showed decreases in the order of 3.5-4 °C (Dickey *et al.*, 1998), or the cases of
37 cyclones Nargis (2008) and Laila (2010), in the Bay of Bengal, that caused SSTs to drop by around 1.76 °C (Maneesha
38 *et al.*, 2012). Additionally, several model-based works focused on either the effects caused by the TCs, or the
39 interaction of the TC with its own cold wake (e.g., Chen *et al.*, 2017; Zhang *et al.*, 2019).

40 There are also biological responses to the passage of a TC. Due to the upwelling of colder water, transport of nutrient-
41 rich water from the sub-superficial layer may also occur (Kawai and Wada, 2011). In this case, phytoplankton can
42 quickly increase in the surface layer following the rise in nutrients. This increase can be remotely sensed through
43 satellite observations that capture the chlorophyll-a concentration (Chl-a) increasing after the passage of a TC, since
44 Chl-a is generally accepted as a proxy for biological activity (Kawai and Wada, 2011; Liu *et al.*, 2009; Subrahmanyam
45 *et al.*, 2002; Walker *et al.*, 2005).

46 The oceanic response, either physical or biological, to the passage of a TC depends on various aspects, most
47 remarkably the TC's intensity and its translation speed but also the oceanic subsurface conditions (Zheng *et al.*, 2008).
48 The magnitude and significance of these aspects on the modulation of the oceanic response vary regionally, although
49 it is generally regarded that the most impactful phenomena are intense and slow TCs (Chacko, 2019; Price, 1981;
50 Price *et al.*, 1994). Recent studies (e.g., Chacko, 2019; Pan *et al.*, 2018; Shropshire *et al.*, 2016) have shown that
51 regional differences do matter when studying the biological response. In the case of the Bay of Bengal, it was shown
52 that the intensity of a TC is less important, and the most meaningful aspects are the TC's translation speed and, to a
53 lesser degree, a pre-existing shallow mixed layer (Chacko 2019). The results from this study are important to stress
54 that relatively weaker TCs can also induce a strong biological response after their passage.

55 Until now, the Azores region has not been studied regarding its thermodynamic and biological impacts. This section
56 of the North Atlantic basin presents much fewer and weaker cyclones than the tropical band of the basin, with this
57 region being mainly a zone where TCs undergo either cyclosis or post-tropical transition into extra-tropical cyclones
58 or mid-latitude storms (Baatsen *et al.*, 2015; Haarsma *et al.*, 2013). The north-eastern Atlantic (NEA) basin, where the
59 Azores archipelago is located, presents significantly less TCs than the western counterpart, closer to the USA coast
60 (Baatsen *et al.*, 2015; Lima *et al.*, 2021; Haarsma *et al.*, 2013). However, there is growing evidence of a significant
61 increase in the frequency of strong TCs in both western (Kossin *et al.*, 2020) and eastern (Lima *et al.*, 2021) halves of
62 the north Atlantic Ocean. The climatology of the area points to a south-north gradient in both SST and Chl-a, with a
63 decrease in the former and an increase in the latter (Amorim *et al.*, 2017; Caldeira and Reis, 2017). In general, the
64 southern part of the Azores region offers SSTs high enough to maintain TCs, although the necessary atmospheric
65 conditions (e.g., high lapse rates and low wind shear) need to occur for their passage northeast through the Azores

66 (Lima et al., 2021). However, this area is undergoing a transition due to anthropogenic climate change and an increase
67 both in number and intensity of TCs is expected (Baatsen et al., 2015; Haarsma et al., 2013). Therefore, the NEA basin
68 is a challenging study region to assess the impact that lower intensity TCs have on the oceanic surface.

69 The main aim of this study is to analyse in detail the upper ocean response observed after the passage of a TC in the
70 Azores region, which is characterised by its lower-than-normal cyclonic activity in relation to the rest of the north
71 Atlantic basin. In particular, we aim to evaluate the impacts on SST and Chl-a concentration produced by important
72 TC characteristics (averaged maximum wind speed, average translation speed, overall impacted area, time of
73 occurrence, and geometry of the track). Two practical case studies, relative to Nadine (2012) and Ophelia (2017) are
74 then thoroughly analysed to reflect the drawn conclusions for this area.

75 **Data**

76 The main data used to evaluate the oceanic response in this study is divided into three main parts: Remotely sensed
77 interpolated data used to characterise the Chl-a and SST, respectively, and TC track data, which provides the necessary
78 additional information on the location and dynamic variables of each TC, that allow to explore the oceanic response
79 in the aforementioned data. Additionally, non-interpolated datasets are used for the case studies to validate the
80 interpolated ones; and wind-stress data is used for the Hurricane Ophelia study case.

81 Biological oceanic response was evaluated using a multi-sensor daily Chl-a product available through the Copernicus
82 Marine Environment Monitoring Service (CMEMS) in a 4 km x 4 km resolution from the end of 1997 to the present
83 (CMEMS, 2021b). This product, delivered by the ACRI-ST company, is based on the Copernicus-GlobColour project
84 and obtained by merging different sensors: SeaWiFS, MODIS, MERIS, VIIRS-SNPP&JPSS1, OLCI-S3A&S3B. The
85 final Chl-a product is a mix of several algorithms that consider different water conditions, such as oligotrophic,
86 mesotrophic, coastal, clear, and complex waters (Garnesson et al., 2019). To produce a “cloud free” product, the
87 resulting data was subjected to daily interpolation to fill any gaps (Krasnopolsky et al., 2016; Saulquin et al., 2019).
88 The lack of gaps in this dataset is particularly relevant in the context of this study since the areas analysed will be
89 concentrated around the TCs; it is then expected that large amounts of the analysed areas would be under cloud
90 coverage and, therefore, some of the analysed data is not real but interpolated values. Nonetheless, CMEMS provides
91 approximate uncertainty levels for this data, which we used to assess the quality of our results. For further validation
92 purposes we used also a non-interpolated Chl-a product generated by the Ocean Colour component of the European
93 Space Agency’s Climate Change Initiative project (OC-CCI) (Sathyendranath et al., 2019). This dataset results from
94 a merge of several sensors: SeaWiFS LAC and GAC, MODIS Aqua, MERIS, VIIRS, and OLCI. ESA’s OCC-CI
95 version 5.0 Chl-a product has 0.042° resolution and a daily temporal resolution (Sathyendranath et al., 2021).

96 To evaluate the physical oceanic response and to relate this to the biological one, a daily SST dataset from the CMEMS
97 was used, with a 0.05° resolution. This data is available from 1981 up to the near present (CMEMS, 2021a). Similarly
98 to the previous CMEMS interpolated Chl-a product, the SST field is also a blended gap-free analysis product, with
99 the present one resulting from re-processed (A)ATSR, SLSTR and AVHRR sensor data being applied to the

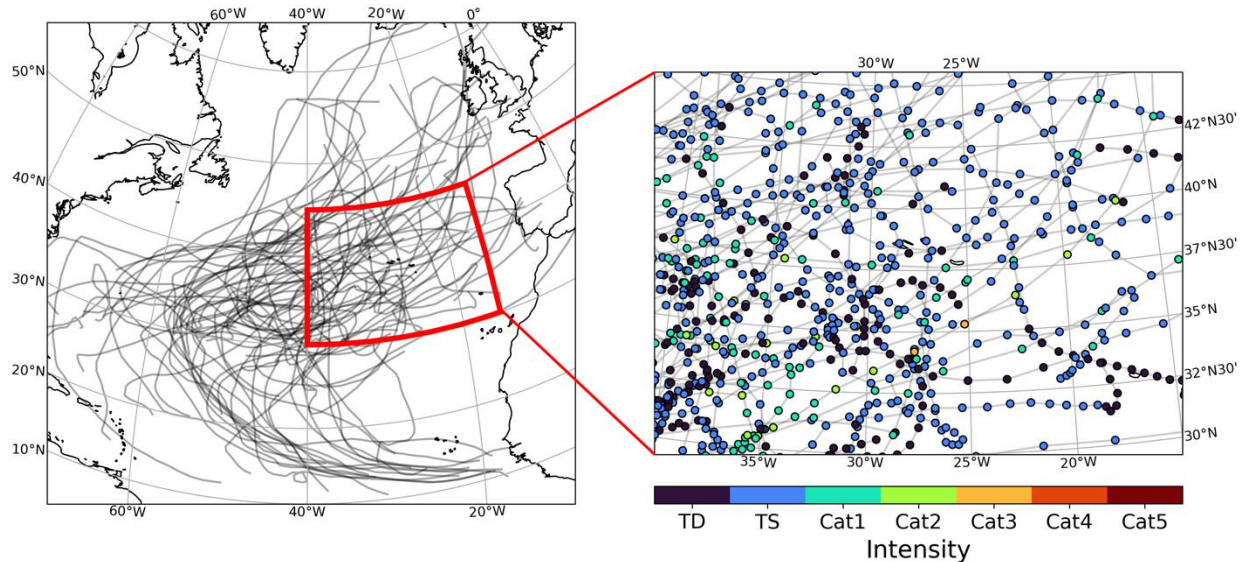
100 Operational SST and Sea Ice Analysis (OSTIA) system (Donlon et al., 2012). This reprocessed analysis product
101 provides an estimate of the SST at 20 cm depth. The inputs to the system are SSTs at 10:30 am and 10.30 pm local
102 time which means that the analyses roughly correspond to the daily average SST (Good et al., 2020; Lavergne et al.,
103 2019; Merchant et al., 2013). As stated before, approximated error values for SST are also provided by CMEMS.
104 Additionally, AVHRR Pathfinder version 5.3 collated data was used as non-interpolated data for validation. This
105 dataset, similarly to the CMEMS one, is a collection of twice daily (averaged to daily), 4 km spatial resolution, merged
106 SST product, provided by NOAA's National Centers for Environmental Information (Saha et al., 2018). The merge
107 of this data, however, is only used to spatially collate the data, as it is a single instrument measurement (AVHRR)
108 onboard NOAA-7 through NOAA-19 Polar Operational Environmental Satellites (POES).

109 Wind stress data to assist in the analysis of the Hurricane Ophelia study case was provided by NOAA's CoastWatch
110 dataset available at https://coastwatch.pfeg.noaa.gov/erddap/griddap/erdQMstress1day_LonPM180.html. This dataset
111 is derived from wind measurements obtained from the Advanced Scatterometer (ASCAT) instrument on board
112 EUMETSAT's MetOp satellites (A and B) at a daily 0.25° resolution, from 2013 to the present. ASCAT presents a
113 near all-weather capacity (not affected by clouds), as it operates a frequency in C-band (5.255 GHz), therefore,
114 minimizing the number of missing values in predominately clouded areas such as the case of TC paths.

115 The TC track data is made available by the *International Best Track Archive for Climate Stewardship Project* version
116 4 (IBTrACS v4) free access dataset (Knapp *et al.*, 2009). This dataset contains global information regarding TC
117 activity since the 1851 hurricane season up to 2020. It aggregates variables such as TC geographical location,
118 maximum wind speed, minimum sea level pressure, and storm radius estimation based on wind intensity, measured at
119 6-hour intervals (original dataset interpolates for increased resolution, at 3-hour rates, however this interpolation only
120 includes the geographical location). For the 1998-2020 period, the Azores region experienced the passage of 62
121 individual TCs accounting to 642 6-hour observations that are categorised in the following intensities according to the
122 Saffir-Simpson hurricane wind scale (Taylor *et al.*, 2010):

- 123 ● 148 tropical depression observations.
- 124 ● 389 tropical storm observations.
- 125 ● 85 category 1 hurricane observations.
- 126 ● 18 category 2 hurricane observations.
- 127 ● 2 category 3 hurricane observations.

128 The full TC tracks can be better visualised in Fig. 1, with the left panel showing the full track for all these 62 TCs
129 observed in the NA basin for the 1998-2020 period and the right panel showing a zoomed view relative to the
130 considered Azores region. Tropical depression observations (dark blue in Fig. 1, right panel) account for 23 % of the
131 total observations and will not be considered in this study, as they present the lower branch of intensities with winds
132 below the 34-kt (18 m/s) threshold. Therefore, a total of 494 TC 6-hour observations were considered for this study.



133
 134 **Figure 1 - Left panel: North Atlantic basin and the tracks of all the TCs that went through or occurred inside the study**
 135 **region (shown by the red outline). Right panel: Zoom of the previous red outline, with each TC observation marked in**
 136 **different colours for intensity (TD: Tropical Depression; TS: Tropical Storm; Cat1 - Cat5: Hurricane category according**
 137 **to the hurricane Saffir-Simpson wind scale).**

138 Since the interpolated datasets used for most of this study do not share the same time frame and to better encapsulate
 139 full years of data, the timeframe of the present study will be from January 1st of 1998 to December 31st of 2020.
 140 Moreover, while we have extracted all the data described above covering the entire North Atlantic basin, we will focus
 141 on the area around the Azores archipelago, delimited by the 15° W and 40° W meridians and between the 30° N and
 142 the 45° parallels (Fig. 1).

143 **Methodology**

144 The region of study was chosen due to its nature regarding TCs, since it is an area with fewer and less intense tropical
 145 storms (Hart and Evans, 2001; Lima et al., 2021; Ramsay, 2017). Generally, tropical cyclosis and post-tropical
 146 transition occur here (Baatsen et al., 2015; Haarsma et al., 2013). Because of these aspects, it corresponds to a much
 147 less studied area and is a good region to characterise oceanic biophysical effects after the passage of (generally) weaker
 148 TCs at higher-than-tropical latitudes and to compare the obtained results with previous literature.

149 To cope with large amounts of data, the bio-physical response was evaluated within a small area around individual
 150 locations obtained for each TCs' best-track location. For this, we used the approximated quadrant radius given by the
 151 IBTrACS v4 dataset. This dataset provides different types of radii depending on the considered isotach, for this study
 152 we used the 34-kt isotach as it corresponds to the lower-bound for the Tropical Storm status according to the Saffir-
 153 Simpson hurricane wind scale (Taylor et al., 2010). Since the considered area of analysis falls above the 34-kt isotach,
 154 tropical depressions were not considered (exact partition of intensities is given at the beginning of the *Results* section).
 155 There are some missing radii values in the middle of TC tracks and, to correct those, a simple linear regression was

156 applied. To illustrate the application of this methodology we present the study cases in the *results and discussion*
157 section, for hurricanes Ophelia (2017) and Nadine (2012). From inside this area of analysis, we may retrieve the Chl-
158 a concentration and SST at their respective resolution. The analysis inside the considered area was performed using
159 histograms, in which each pixel inside the 34-kt isotach contributes to that TCs histogram.

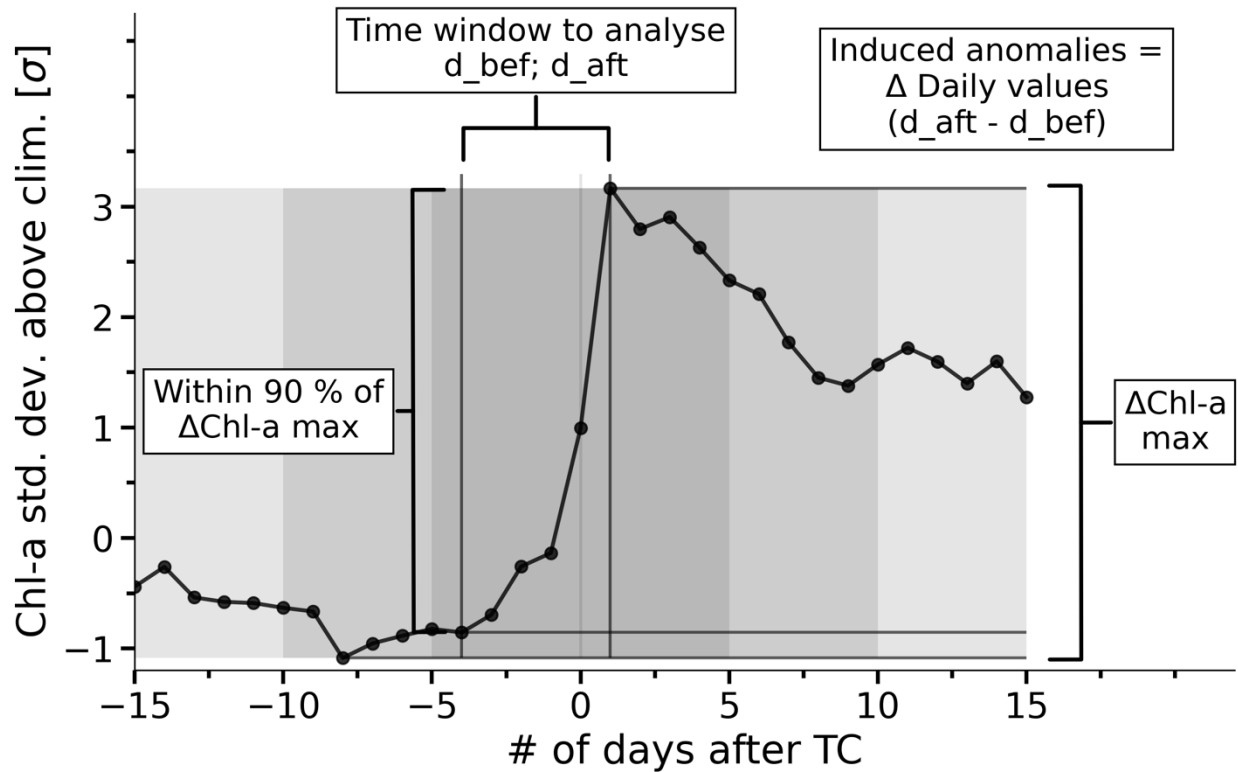
160 To analyse the TCs' impact on their passage, inspiration was taken from Kawai and Wada (2011), who computed the
161 climatic monthly standard deviation of Chl-a on 0.25° grids over a 5-year study period. Here, we compute the daily
162 normalized anomaly from the climatological value (in standard deviation units). For this, we first calculated the
163 climatological mean and associated standard deviation of both Chl-a and SST values for the region that is impacted
164 by each TC on the day of analysis. This is achieved considering the 3 days before and 3 days after the day of analysis,
165 totalling one week that is then retrieved from the entire study period of 22 years, thus ensuring a larger sample and a
166 smoother continuous curve. Then, we compute the mean value in the same area (in which only the TC area was
167 considered) for the day of analysis, and finally, we calculate the normalized anomaly from the climatology on that
168 day. This analysis was performed considering 30 days before and after each TC to allow then the analysis and
169 identification of an ideal window to compute the induced anomalies. To compute this ideal window, we searched for
170 the maximum difference between the number of standard deviations over the climatological value before and after the
171 storm.

172 To compromise between having the maximum difference and ensuring a time window as close as possible to the storm
173 (to minimize external factors to the TC), we performed a sensibility study on the length and location of the considered
174 time window. First, we analyse the overall maximum difference in the 61-day period (including the day of the storm)
175 and then search for a secondary maximum value that is within 10 % of it considering a smaller sample of days,
176 decreasing in groups of 5 days each time this search is made (e.g., the first iteration would be 25 days before and 30
177 after, the second 30 before and 25 after, the third 25 before and after, etc.), until an optimum maximum difference
178 value is identified. With this window defined, the induced (or TC-related) anomalies are simply the difference between
179 the daily values of Chl-a or SST after and before the TC.

180 As an example of this methodology, Fig. 2 shows the Chl-a standard deviation over the climatological value in the
181 case of Hurricane Nadine. In this case, only 15 days around the TC are shown for clarity. We can see that the maximum
182 difference is obtained between 8 days before and 1 day after the storm ($\Delta\text{Chl-a max}$). However, when we take into
183 account the compromise of considering windows located as close as possible to the occurrence of the TC over the
184 region, we see that the value found between 4 days before and 1 day after is within 10 % of the absolute maximum.
185 This methodology is then applied to all 6-hour observations individually and for each TC, thus resulting in two groups
186 of induced anomalies (per TC and per 6-hour observations) where we can study these with respect to the TCs averaged
187 (per TC) or instantaneous (6-observations) characteristics.

188 To address the possibility that some pixels are overlaid on top of each other, which would contaminate the analysis,
189 as observed in the case of the slow erratic Hurricane Nadine (presented in the *results and discussion* section as a study
190 case), we did not take into consideration the days in which the TC is over the aforementioned overlaid region. In the

191 case of these pixels, the day considered to be after the TC is the day after it has completely passed over the area (i.e.,
 192 the observations in that pixel during the days the TC is still over the area are discarded). However, when we consider
 193 independent 6-hour observations, this caveat cannot be accounted for since we have no way of knowing if that area
 194 has been influenced or not by the TC before, for how long, or even if a future observation will impact the area.



195
 196 **Figure 2 - Schematic of the applied methodology for each TC. Black line shows the number of standard deviations from the**
 197 **climatological values for the area surrounding Hurricane Nadine. A detailed description of this methodology can be found**
 198 **in the text.**

199 As previously mentioned in the *Data* section, the interpolated data used for this study is expected to encounter some
 200 regions where clouds are to be expected due to the presence of the TCs. To account for this potential caveat, we looked
 201 at the uncertainties associated with the data before and after the TCs, as well as during the TC (e.g., day 0 in Fig. 2),
 202 to evaluate if there were clear increases in uncertainty for cloud covered situations.

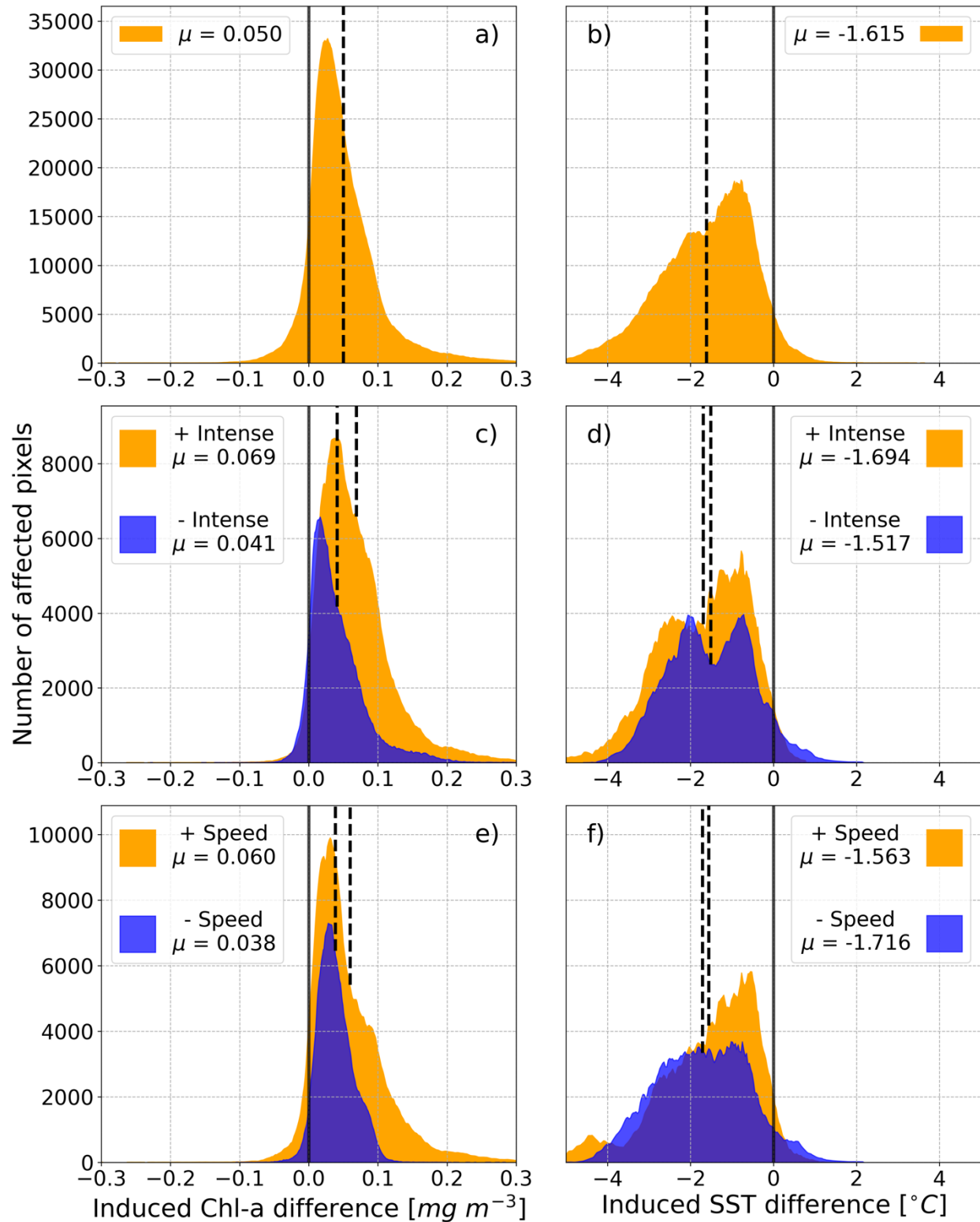
203 Two case studies were looked at in greater detail: Hurricane Ophelia (2017) and Hurricane Nadine (2012). The former
 204 was performed to assess the different impacts along the lifecycle of the storm, and different histograms were produced
 205 for smaller portions of the TC. The latter was made to analyse the possible increasing impacts the storm geometry
 206 could cause. Additionally, these study cases were used as validation for the interpolated “cloud-free” data, where a
 207 comparison was made between the non-interpolated and the interpolated “cloud-free” data described in the *Data*
 208 section.

209 **Results and Discussion**

210 Applying the mentioned methodology leaves us with a large pool of induced anomalies, from which we can now
211 evaluate the distribution of these TC-related anomalies for both the Chl-a and SST as shown in Figs. 3a and 3b in the
212 form of histograms of induced Chl-a and SST induced anomalies, respectively. Both variables present a large impact
213 after the passage of TCs, with the Chl-a presenting a mean response of positive 0.050 mg m^{-3} and the SST showing a
214 mean response of $-1.615 \text{ }^\circ\text{C}$. Figs. 3c-f show the corresponding distributions as a function of the cyclone's intensities
215 (Figs. 3c and 3d) and translation speeds (Figs. 3e and 3f). To make these distinctions, we chose only the high values
216 (either regarding intensity or translation speed) to be those above the third quartile and the lower values to be those
217 below the second quartile.

218 Firstly, regarding intensity (Figs. 3c and 3d), we have the induced response of the most powerful intensities in orange
219 and the weaker ones in blue. Regarding the impact as a function of intensity it is possible to observe that more powerful
220 TCs tend to induce a stronger biological response than weaker ones, which have a mean response closer to zero. It is
221 also important to note that the more powerful TCs have a response that is much more skewed towards extreme positive
222 values of Chl-a. Fig. 3d also shows a great impact regarding different intensities in SST, in which even weaker TCs
223 show a substantial mean response of $-1.517 \text{ }^\circ\text{C}$ and nearly all the analysed pixels showing negative induced anomalies.
224 Important to note the nearly bimodal nature of this distribution, which can be attributed to both the earlier phase of
225 TCs (more energy being drawn from the ocean) resulting in more negative SST values, and the less negative
226 corresponding to the later part of TCs since baroclinic instabilities are more prevalent than the action of moist enthalpy
227 flux from the ocean at this phase (Baatsen et al., 2015; Emanuel, 2003). Powerful TCs induced a more varied
228 distribution of induced anomalies, with a mean response of $-1.694 \text{ }^\circ\text{C}$.

229 Regarding the different translation speeds, Fig. 3e shows that, for biological responses, faster TCs show a greater
230 mean value of $+0.060 \text{ mg m}^{-3}$. This difference is not as remarkable as the one in Fig. 3c. On the other hand, the SST
231 response (Fig. 3f) seems to be weakly impacted by the TC's translation speed, with slower TCs having a slightly
232 stronger impact than faster ones, while the mean response values do not differ as much as the ones in Fig. 3d.
233 Additionally, even if faster TCs do not affect the SST response as much as slower ones, the mean value is still close
234 to what is seen in the general case in Fig. 3b, and most of the impact is towards negative SSTs.

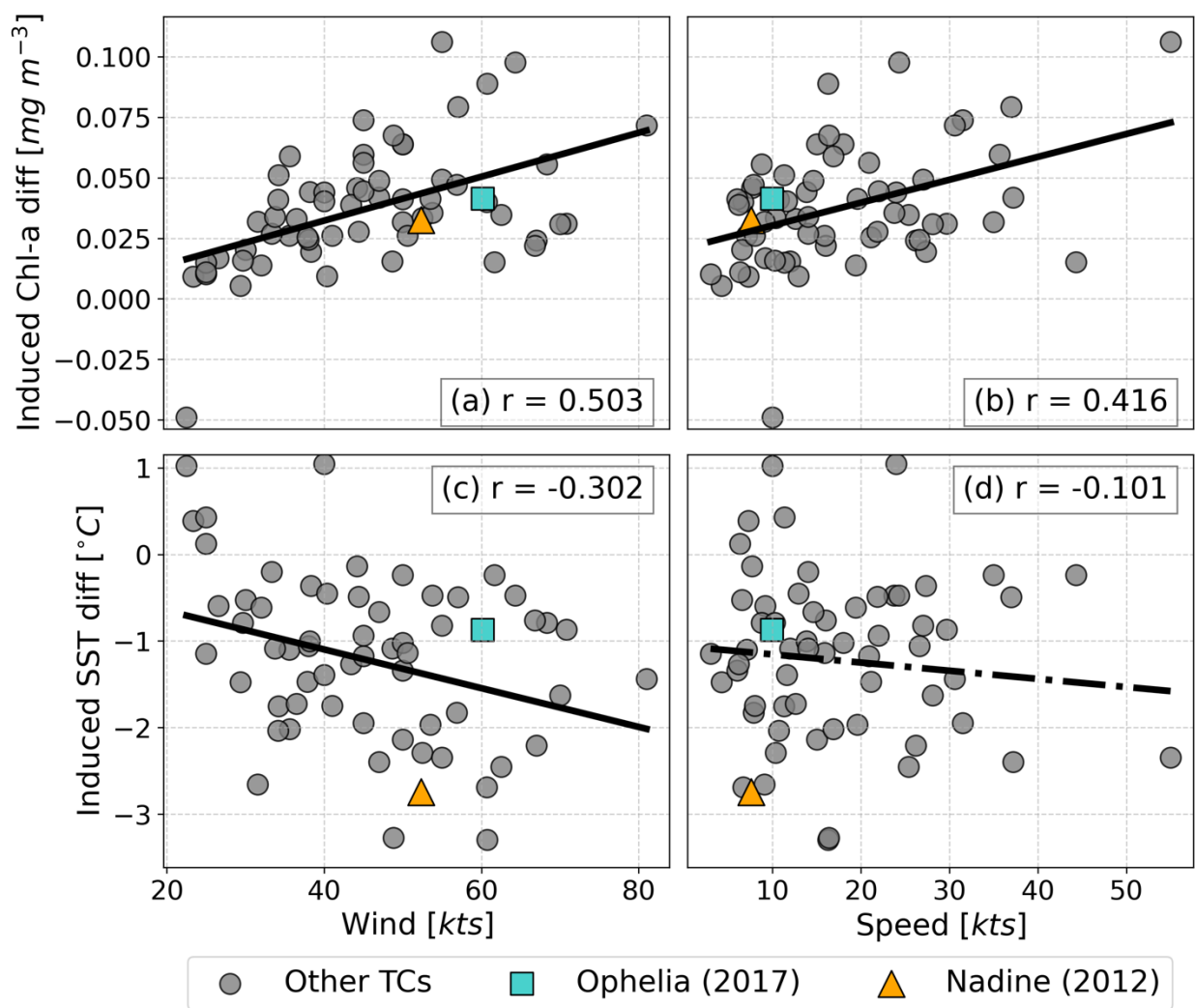


235

236 **Figure 3 - Histograms for the: a) Total Chl-a and b) SST induced anomalies; c) Chl-a and d) SST induced anomalies after**
 237 **weak (blue) and powerful TCs (orange); e) Chl-a and f) SST induced anomalies after slow TCs (blue) and fast TCs (orange).**

238 Each subplot histogram presents the respective population mean value (μ) in a dashed black line, and the zero value in a
 239 grey line.

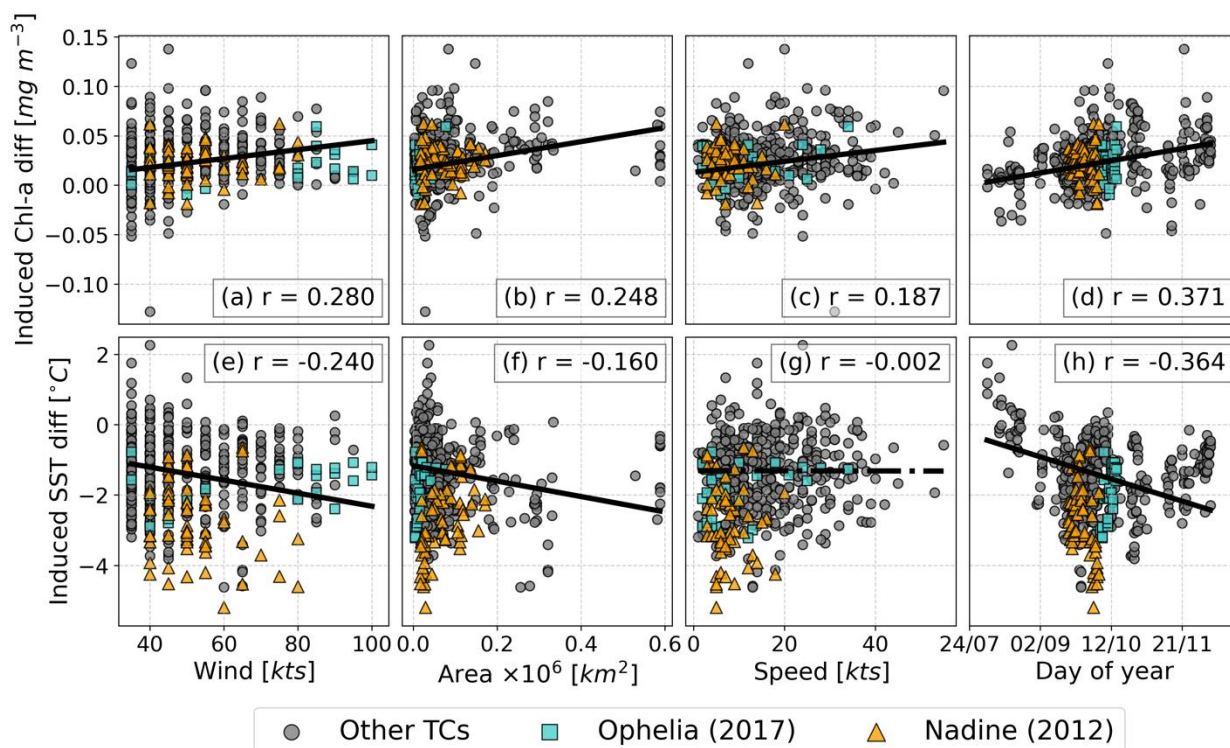
240 To quantify these relations, Fig. 4 shows the storm-averaged induced anomalies compared to the averaged maximum
 241 wind and average translation speed. The linear regression is also shown for each of the comparisons, with nearly all
 242 results significant at the 95 % statistical level. According to these plots, only the translation speed in relation to the
 243 SST induced anomalies (Figs. 4d) did not show a significant relation at the 95 % statistical confidence level (marked
 244 by the dashed regression line). Regarding the mean wind (Figs. 4a and 4c), and therefore the TC's average intensity
 245 within the Azores region, the linear regression showed significant values, upwards of 0.5 for Chl-a and -0.3 for SST
 246 induced anomalies. In the case of Chl-a, like observed in Fig. 3, the relation is positive while with SST this relation is
 247 negative. Considering the translation speed, the relation is equally positive and significant for biological responses (r
 248 = 0.416).



249
 250 **Figure 4 - Linear regression of Chl-a (top panel) and SST (bottom panel) induced anomalies for each TC, respectively, when**
 251 **compared with average winds in knots (left column); and average TC translation speed in knots (right column). In each**

252 plot the Pearson R is presented, and the regression's significance is marked by the type of line used in the regression, with
 253 a dashed line representing non-significant at a 95 % confidence level, and a solid line representing a regression significant
 254 at the 95 % confidence level.

255 Further analysis of other TC characteristics requires a different approach. Fig. 5 shows similar relations to Fig. 4 but
 256 considering 6-hour observations instead of total TC mean values. This is made to account for the possible error that
 257 averaging a whole TC may create since the cyclone's characteristics may change substantially along its lifetime. This
 258 analysis, however, does not consider the possibility of superposition in pixels from observation to observation – i.e.,
 259 from a TC that either moves slowly or whose track is more erratic, ending up covering the same area for several
 260 hours/days. This caveat was not present in Fig. 4 since we considered the TC lifetime as a whole and could then
 261 disregard the days of superposition. Using 6-hour observations, we can study several types of characteristics that
 262 change between observations, such as the impact area or the time of season when it occurred, adding to the already
 263 seen maximum wind speed and translation speed.



264
 265 **Figure 5 – Same as in Fig. 5 but considering individual 6-hour observations. Two columns are added: (b) and (f) with respect**
 266 **to the area affected by that observation; and (d) and (h) with respect to the time of the year when that observation occurred.**

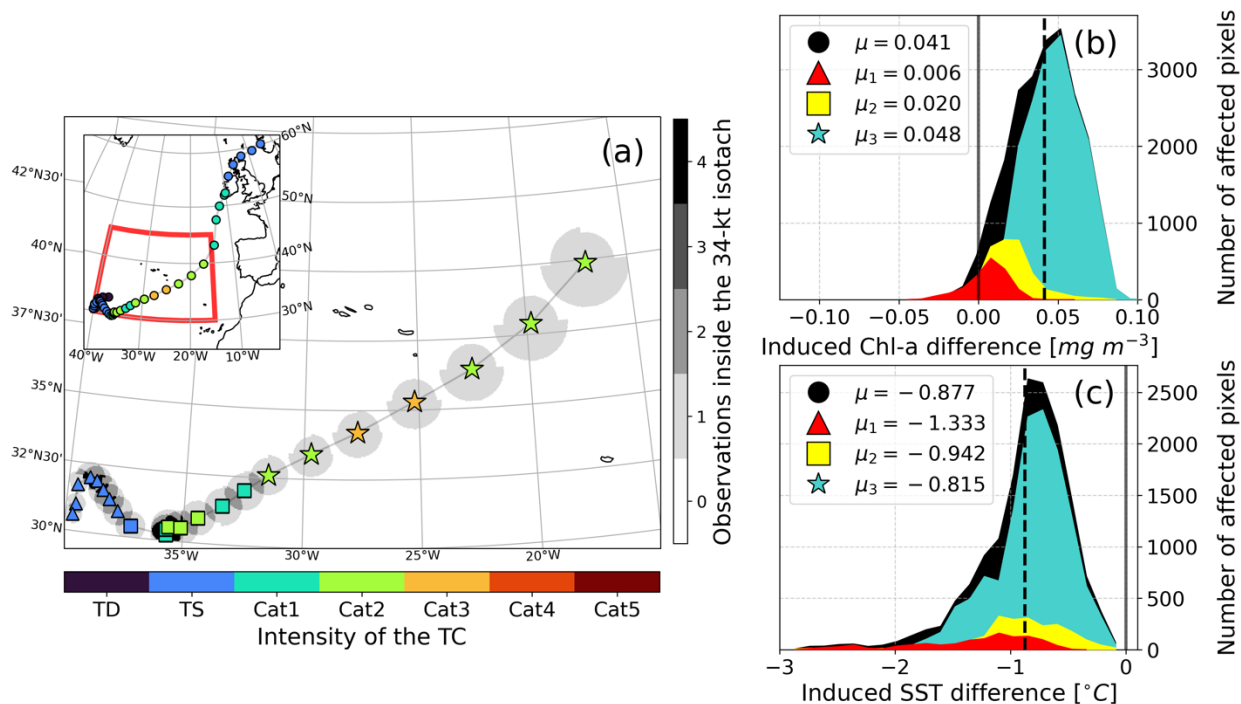
267 Considering then the maximum wind speed per observation (Fig. 5a and 5e), both variables are significantly related
 268 to this characteristic, which is expected considering the analysis made in Figs. 3 and 4. As previously noted in the
 269 form of histograms in Fig. 3, most observations show a positive impact regarding Chl-a and, especially for SST as
 270 most fall below zero, a negative change after a TC. The affected area (Figs. 5b and 5f) also presents a significant
 271 relation, although less intense than that observed with the maximum winds. However, it should be noted that this

272 variable is linked to the mean winds, since more intense cyclones tend to be larger than less powerful ones, but also
273 to the storm phase, since storms nearing their post-tropical transition tend to grow larger (Knaff et al., 2014).
274 Translation speed is the less correlated variable from those studied (Fig. 5c and 5g), with only the biological response
275 seeing a positive relation to this characteristic, agreeing with the previous results from Figs. 3 and 4. The time period
276 in the season in which the TC occurs seems to also be important for the magnitude of the average induced anomaly
277 seen in both variables (Figs. 5d and 5h) with late occurrences in the season showing greater responses respective to
278 the signal of induced anomalies seen in Figs. 3a and 3b. Lastly, a geographical correlation was concluded not to be
279 relevant for this study (not shown), as both variables were correlated with both latitude and longitude, and only non-
280 significant relations were found.

281 The results presented so far in this study result from interpolated “cloud-free” data and should be quality assured to
282 guarantee the integrity of the conclusions made previously. As mentioned in the *Data* section, CMEMS provides
283 measures of uncertainty for the used Chl-a and SST datasets. Thus, we have explored these values at different periods
284 as a first step in validating the quality of the data. Figure S1 shows the associated uncertainty with respect to the
285 absolute observed values both for Chl-a (top panels) and SST (bottom panels) for three different periods surrounding
286 a TC event (before, during, and after), and a randomly drawn sample of the same size as the data analysed in the other
287 subplots. It becomes immediately clear from these plots the considerably different magnitude of uncertainty for this
288 data, with Chl-a (Figs. S1a-d) ranging from 25 % to 45 % considering all moments, while SST (Fig. S1e-h) does not
289 commonly surpass 0.4 % with a mean error around the 0.25 %. The randomly drawn sample of data gives a rough
290 idea of the average uncertainty we can find in this dataset, with Chl-a (Fig. S1a) presenting values around 35 % and
291 SST (Fig. S1e) around 0.25 %. Additionally, we should consider three distinct moments of analysis, namely before
292 and after the TC passage, which corresponds to the data used to compute the induced anomalies, and during the TCs,
293 which should be the moment with most cloud-cover over the studied regions. Looking first at Chl-a (Figs. S1b-d) we
294 see the progression from near normal uncertainty before the TC (Fig. S1b) to an increase during TCs (Figs. S1c),
295 likely due to the larger cloud-covered area in that situation. After the storm (Fig. S1d) however, the uncertainty
296 substantially decreases reaching values below the randomly drawn sample (around 30 % compared to 35 %). For the
297 SST (Figs. S1f-h), the associated uncertainty does not fluctuate substantially, constantly being below the 0.3 % mark.
298 Additionally, the variation that has been identified before, with Chl-a increasing and the SST decreasing, is noticeable
299 in both variables.

300 Visible in Figs. 4 and 5 are two case studies: Hurricane Ophelia in 2017 (squares) and Hurricane Nadine in 2012
301 (triangles). These case studies were chosen based on the presented characteristics, coupled with the amount of
302 sampling data within the region. Hurricane Ophelia (2017) was chosen due to its large intensity in the region (squares,
303 Fig. 4 and 5), reaching a category 3 intensity in the Saffir-Simpson hurricane wind scale, something abnormal for the
304 region (Lima *et al.*, 2021). The complete TC track can be seen in Fig. 6a insert. Besides the large intensity, Ophelia’s
305 genesis took place inside our study region which enabled us to study different phases of the storm and its impacts on
306 the ocean surface in the region. Even though hurricane Ophelia was so intense, this storm impacted a very small area
307 (Figs. 5b and 5f) particularly when compared with the other case study, Hurricane Nadine (2012). Hurricane Nadine

308 (Fig. 7a) was chosen due to its large sampling, relatively high intensity (maximum category 1) and great impact area
 309 (second highest in this study, considering cumulative area of impact). The large impacted area was amplified by the
 310 geometry of the storm's track (i.e., many overlaid observations). Only the final stage of Hurricane Nadine was caught
 311 within the study region, producing an ideal case study to analyse the impact of a less intense storm that heavily
 312 impacted a particular region due to its geometry.

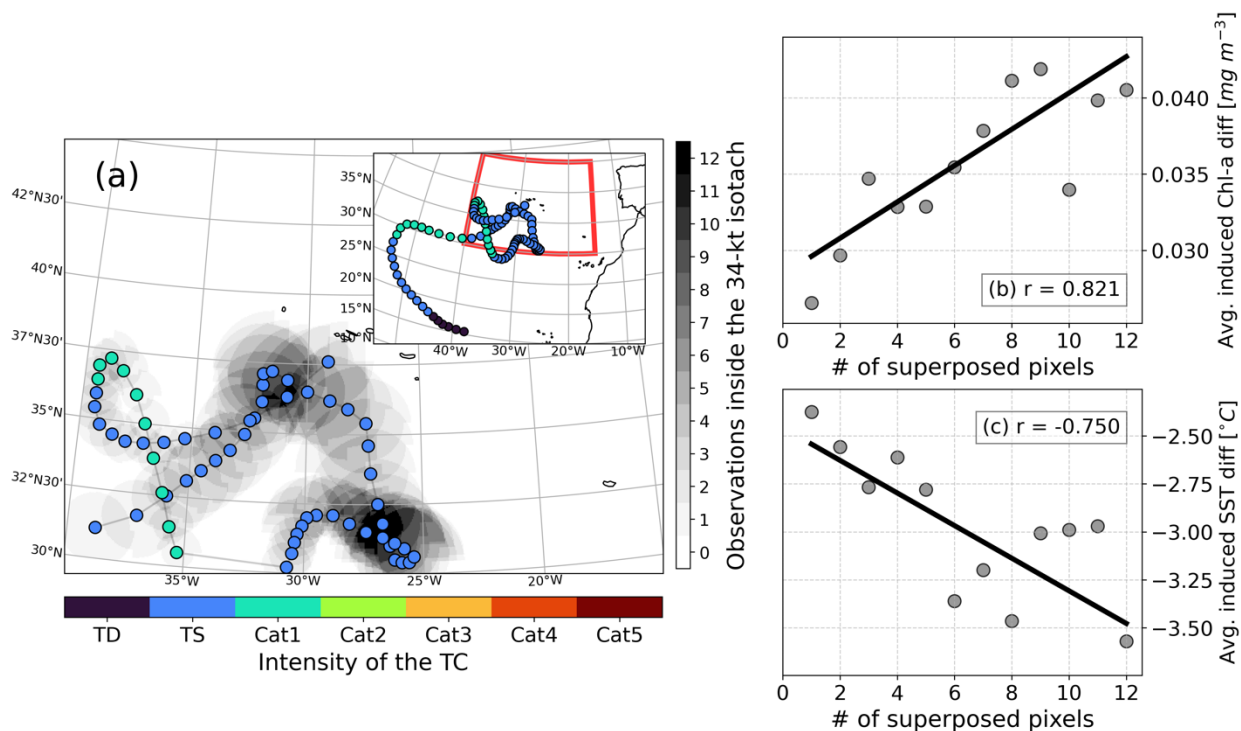


313
 314 **Figure 6 - Case study for Hurricane Ophelia, in 2017, with its track on the left panel (scatter marker colour scheme**
 315 **represents intensity as in Fig. 1), as well as the affected area around the cyclone (marked as the 34-kt isotach**
 316 **according to the number of pixels overlapping. Inside, there is an inset with the full track and the region of study**
 317 **marked with a red box. Ophelia track is divided in three phases: Histograms show induced Chl-a (b) and SST induced anomalies**
 318 **(c), by phase of the storm (colours) and in total (black). The phase of the storm is marked in (a) as triangles (genesis),**
 319 **squares (maturing), and stars (mature) and correspond to the colours in (b) and (c).**

320 For the case study of Hurricane Ophelia (2017), three different phases of the storm were studied, corresponding
 321 approximately to: cyclogenesis (Fig. 6a, triangles), maturing (Fig. 6a, squares), and mature hurricane (Fig. 6a, stars).
 322 There are 23 total observations; the first two phases encompass 8 observations and the last one 7. Each of these phases
 323 has its own histogram in Figs. 6b and 6c (shown in colours), for the induced Chl-a and SST TC-related anomalies,
 324 respectively. The histograms are inserted in a larger one (in black), representing the total induced anomalies caused
 325 by Ophelia and therefore, the sum of all three phases will result in the bigger histogram. Regarding the Chl-a induced
 326 anomalies (Fig. 6b), Ophelia seemed to have a higher impact towards the end of its track in the region of study, when
 327 the storm had the highest intensity and the mean values of the induced anomalies increased along the track. Even at
 328 the storm's genesis, the induced anomalies were mostly positive with a mean value of $+0.006 \text{ mg m}^{-3}$ reaching $+0.048$
 329 mg m^{-3} in the most intense phase. In contrast, the SST induced anomalies (Fig. 6c) present the highest mean response

330 (-1.333 °C) at the initial phase. The SST induced anomaly is then seen decreasing as the storm goes on, with the last
 331 phase weighing the most in the general distribution (as was seen for the Chl-a). The highest SST impact of the storm
 332 during the initial phases may reflect that this is the phase of the storm with highest interaction with the ocean, regarding
 333 thermodynamic exchanges (Emanuel, 2003).

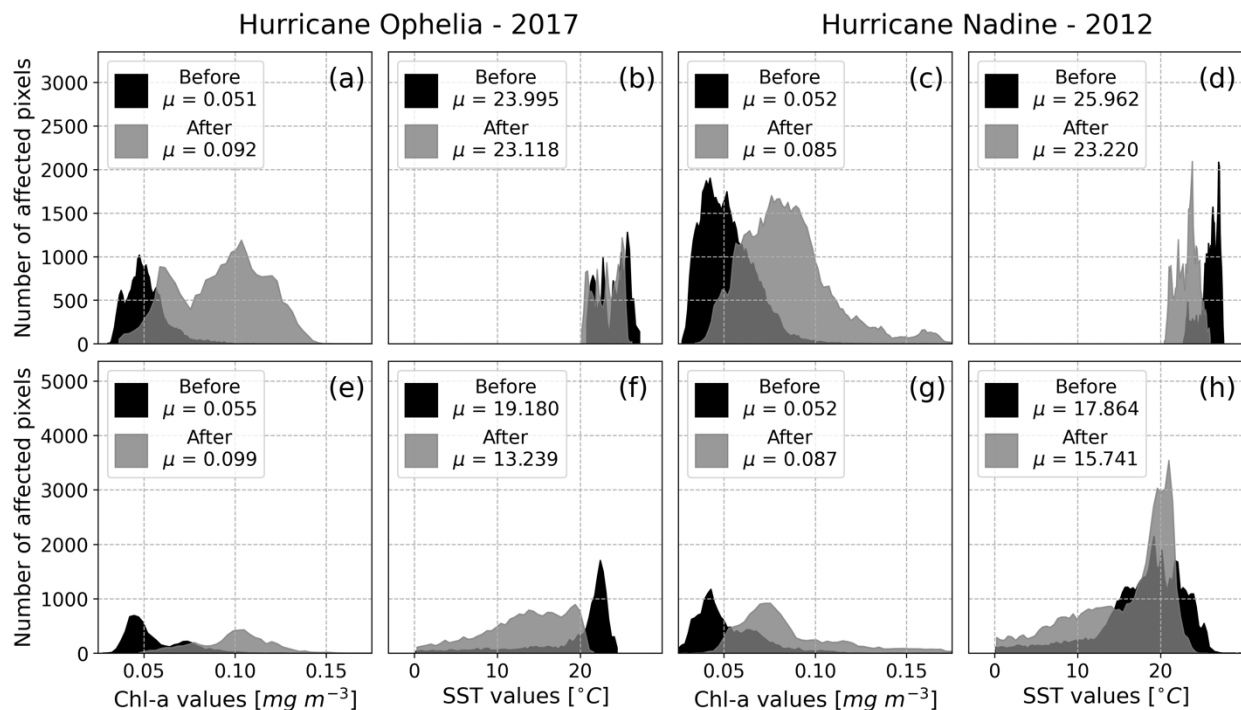
334 As a further insight to Ophelia’s interaction with the ocean surface, Fig. S2 shows the mean modulus of wind stress
 335 on the surface, by day of analysis (Fig. S2a) and by Ophelia’s 6-hour observations (Fig. S2b). Marked in both these
 336 plots are the analysed periods in corresponding colours and marker type to Fig. 6. These plots exceed the original
 337 study region, in order to fully encompass the TCs entire lifetime. There is a significant relation between the increased
 338 mean modulus of the wind stress and the evolution of the TC in time. This increase may be related to the increase in
 339 the storm’s intensity. As Ophelia reaches its maximum intensity, so does the observed interaction with the ocean,
 340 decreasing afterwards as the storm moves north-eastward and undergoes post-tropical transition. This observed
 341 interaction with the ocean might be the reason for the maximum induced anomaly of Chl-a being observed at the end
 342 of Ophelia’s passage over the study region, inducing the mixing of the superficial layer.



343
 344 **Figure 7 - Case study for Hurricane Nadine, in 2012, with the left panel the same as in Fig. 6. For Nadine, plots (b) and (c)**
 345 **pertain to the average induced Chl-a and SST induced anomalies, respectively, based on the amount of superposition**
 346 **verified in each pixel.**

347 Hurricane Nadine’s (2012) case study shows very different behaviour and impact during its lifetime to that of
 348 Hurricane Ophelia. In this case, we present scatter plots of the averaged induced anomalies for the areas (Figs. 7b and
 349 7c) corresponding to the superposition of pixels, i.e., the number of repeated observations inside the 34-kt due

350 to storms track geometry (as seen in Fig. 7a). The conclusions drawn regarding the Chl-a and SST induced anomalies
 351 are similar and significant in this case study: The more time the TC spent over a certain area the more this area became
 352 affected by its passage, with large TC-related anomalies registered in both variables compared to less superposed ones
 353 (over 0.040 mg m^{-3} and $-3.500 \text{ }^{\circ}\text{C}$ for Chl-a and SST, respectively at 12 superposed pixels), and all cases being positive
 354 (negative), for Chl-a (SST). It is possible to hypothesise that the translation speed also had a relevant role in these
 355 results, with a slower TC (Nadine was one of the slowest TCs in this study, as seen by the closer observations in Fig.
 356 7a and by Figs. 4 and 5) spending more time over a region and therefore producing larger induced anomalies.



357
 358 **Figure 8 – Comparison between interpolated “cloud-free” data (top row), and non-interpolated data (bottom row), for**
 359 **Hurricanes Ophelia (2017) and Nadine (2012). Values for non-interpolated data were obtained with the same methodology**
 360 **as the ones presented before and represent the exact same days of analysis. Mean values for each histogram are presented,**
 361 **with black histograms representing the situation before the TC and the grey ones the situation after.**

362 For these two case studies, we considered an additional quality assessment exercise, by comparing the interpolated
 363 “cloud-free” data to similar non-interpolated datasets. Figure 8 shows the histograms obtained for Ophelia and Nadine
 364 for the situations before and after the TC, independently, since non-interpolated data cannot be correctly subtracted as
 365 corresponding pixels may not be available. Overall, and despite the different number of observations considered, the
 366 Chl-a presents the same average response between the different types of data for both TCs, with non-interpolated data
 367 having an observed mean increase of 0.044 mg m^{-3} for Ophelia (Fig. 8e) compared to 0.041 mg m^{-3} for interpolated
 368 data (Fig. 8a), with these values representing the difference in the mean values shown in Fig. 8. Likewise, non-
 369 interpolated data reveals an increase of 0.035 mg m^{-3} for Nadine (Fig. 8g), compared to 0.033 mg m^{-3} for interpolated
 370 data (Fig. 8c). Looking at the histograms, the shape of the data itself does not differ much between the different types,

371 with peaks more or less located over the same values and distributions ranging the same values. However, for the SST
372 variable, despite both TCs presenting relatively similar decreases between both types of data, the non-interpolated
373 data has a wider range of values, and the peaks do not correspond so closely. This, however, may be due to the process
374 of data collation. In this process, some pixels are averaged with incorrect ones, resulting in unrealistic values in some
375 areas. This can be identified by the unrealistic SST seen in Figs. 8f and 8h, with values that do not support TC
376 development around 18-19°C and, so far as reaching 0°C. Nonetheless, interpolated SST data does show very low
377 uncertainty as verified before (Fig. S1).

378 **Final remarks**

379 The current study provides the first general assessment of the bio-physical oceanic response to the passage of TCs in
380 a relatively low cyclonic activity area such as the region near the Azores archipelago. It is important to stress the
381 efficiency of identifying the precise timing and associated spatial impacts of all TCs using remotely sensed products
382 that rely on interpolated areas to fill existing gaps due to cloud coverage or lack of satellite imagery.

383 Over the Azores region, the existence of a bio-physical response after the passage of a TC was identified from the
384 analysis of Chl-a and SST datasets, which produced signatures of positive Chl-a and negative SST induced anomalies.
385 This signature is more intense for the SST analysis, in which the passage of a TC results in nearly all observed pixels
386 to have a negative (i.e., cooling) induced anomaly. On average, TCs produced positive induced anomalies in the order
387 of 0.050 mg m⁻³ regarding Chl-a and a mean SST cooling of 1.615 °C.

388 The more powerful TCs tend to produce more intense bio-physical oceanic responses, which agree with previous
389 literature on the topic (Chacko, 2019; Price, 1981; Price et al., 1994). TC translation speed was also found to be
390 associated with the induced anomalies, although the relationship was found to be positive and significant in the case
391 of Chl-a while it was not significant at the 95 % statistical confidence level for SST. The impacted area was also found
392 to be significantly linked to the oceanic response. However, the sensitivity to the impacted area can rise due to several
393 other factors: slower TCs impact larger areas (due to track geometry); more intense TCs impact larger areas (Knaff et
394 al., 2014); and TCs nearing post-tropical transition are generally larger (Knaff et al., 2014). These effects, either
395 individually or combined, can affect the induced anomalies at different levels. Additionally, the oceanic response was
396 found to be larger later in the season, with significant relation in both variables. This may be due to the seasonal
397 variability itself, as the normal climatological values for that time of the year are not seen during exceptional TC
398 conditions (e.g. SST is usually colder but TC prone conditions require it to be higher) (Amorim et al., 2017; Lima et
399 al., 2021) and the oceanic response may help the impacted area return to values closer to the climatology, in both
400 variables, in respect to that time of the year.

401 Two particular case studies were evaluated in further detail concerning hurricanes Ophelia (2017) and Nadine (2012).
402 Hurricane Ophelia was a particular case as it corresponds to the only major hurricane in this study region and had
403 almost its entire track inside this area. Ophelia showed strong induced anomalies for both Chl-a and SST variables.
404 Regarding Chl-a, Ophelia had a stronger impact towards the end of its track within the region, revealing that its
405 intensity played a key role in inducing Chl-a TC-related anomalies, with the mean modulus of wind stress revealing a

406 positive and significative relation to the evolution of the storm and therefore its intensity. On the other hand, Ophelia
407 had a stronger impact on the SST in its cyclogenesis, probably related to ocean-atmosphere thermodynamic exchanges
408 during its maturing. Hurricane Nadine, one of the slowest TCs in this study, showed more prominent induced
409 anomalies, especially regarding SST. In this case, considering the low translational speed of Nadine, the objective was
410 to study the impact that consecutive overlaid observations had on the induced anomalies. It is evident through this
411 analysis that the impact increases with the number of superposed observations, implying that Nadine’s slow translation
412 speed and particular track geometry played a key role in creating such TC-related anomalies.

413 This study allowed for both the quality control of the remotely sensed “cloud-free” Chl-a and SST multi-sensor
414 products by comparing them to similar non-interpolated products, and in the sense that it identified expected changes
415 in the variables in areas covered by TC clouds and established crucial relations with some principal TC aspects. Future
416 studies should aim to understand the inherent physical mechanisms that affect the ocean during and after the passage
417 of a TC to better comprehend the associated induced anomalies.

418 **Code and Data availability**

419 All code and raw data used to support the conclusion of this article will be made available by the authors, without
420 undue reservation.

421 **Acknowledgements**

422 Research by Miguel M. Lima was supported by the Portuguese Science Foundation (FCT) through the project
423 “DiscoverAZORES”, PTDC/CTA-AMB/28511/2017. The authors would like to thank the anonymous reviewers for
424 their thoughtful comments, suggestions, and efforts towards improving this work.

425 **Author Contribution**

426 Miguel M. Lima: Conceptualization, methodology, software, validation, formal analysis, investigation, writing –
427 original draft, review and editing. Célia M. Gouveia: Validation, supervision, writing – review and editing. Ricardo
428 M. Trigo: Validation, supervision, writing – review and editing, funding acquisition.

429 **Declaration of Interests**

430 The authors declare that they have no known competing financial interests or personal relationships that could have
431 appeared to influence the work reported in this paper.

432 **References**

433 Amorim, P., Perán, A. D., Pham, C. K., Juliano, M., Cardigos, F., Tempera, F., and Morato, T.: Overview of the
434 ocean climatology and its variability in the Azores region of the North Atlantic including environmental
435 characteristics at the seabed, *Frontiers in Marine Science*, 4, 56, doi:10.3389/fmars.2017.00056, 2017.

436 Baatsen, M., Haarsma, R. J., Van Delden, A. J., and de Vries, H.: Severe Autumn Storms in Future Western Europe
437 with a Warmer Atlantic Ocean, *Clim. Dyn*, 45 (3-4), 949–964, doi:10.1007/s00382-014-2329-8, 2015.

438 Caldeira, R., and Reis, J. C.: The Azores confluence zone. *Frontiers in Marine Science*, 4, 37,
439 doi:10.3389/fmars.2017.00037, 2017.

440 Chen, S., Elsberry, R. L., and Harr, P. A.: Modelling interaction of a tropical cyclone with its cold wake, *J. Atmos.*
441 *Sci.*, 74(12), 3981-4001, doi:10.1175/JAS-D-16-0246.1, 2017.

442 Chacko, N.: Differential chlorophyll blooms induced by tropical cyclones and their relation to cyclone
443 characteristics and ocean pre-conditions in the Indian Ocean. *J. Earth Syst. Sci.*, 128(7), 1-11. doi:10.1007/s12040-
444 019-1207-5, 2019.

445 CMEMS: ESA SST CCI and C3S reprocessed sea surface temperature analyses. Retrieved from
446 [https://resources.marine.copernicus.eu/?option=com_csw&view=details&product_id=SST_GLO_SST_L4](https://resources.marine.copernicus.eu/?option=com_csw&view=details&product_id=SST_GLO_SST_L4_REP_OBSERVATIONS_010_024)
447 [_REP_OBSERVATIONS_010_024](https://resources.marine.copernicus.eu/?option=com_csw&view=details&product_id=SST_GLO_SST_L4_REP_OBSERVATIONS_010_024), 2021a.

448 CMEMS: Global ocean chlorophyll, PP and PFT (copernicus-globcolour) from satellite observations: Monthly and
449 daily interpolated (reprocessed from 1997). Retrieved from
450 https://resources.marine.copernicus.eu/?option=com_csw&view=details&product_id=OCEANCOLOUR_GLO_CH
451 [L_L4_REP_OBSERVATIONS_009_082](https://resources.marine.copernicus.eu/?option=com_csw&view=details&product_id=OCEANCOLOUR_GLO_CH_L_L4_REP_OBSERVATIONS_009_082), 2021b.

452 Dickey, T., Frye, D., McNeil, J., Manov, D., Nelson, N., Sigurdson, D., ... and Johnson, R.: Upper-ocean
453 temperature response to Hurricane Felix as measured by the Bermuda Testbed Mooring, *Mon. Weather Rev.*,
454 126(5), 1195-1201, doi:10.1175/1520-0493(1998)126<1195:UOTRTH>2.0.CO;2, 1998.

455 Donlon, C. J., Martin, M., Stark, J., Roberts-Jones, J., Fiedler, E., and Wimmer, W.: The operational sea surface
456 temperature and sea ice analysis (OSTIA) system, *Proc. SPIE*, 116, 140-158, doi:10.1016/j.rse.2010.10.017, 2012.

457 Emanuel, K., Tropical Cyclones. *Annu. Rev. Earth Pl. Sc.*, 31 (1), 75–104,
458 doi:10.1146/annurev.earth.31.100901.141259, 2003.

459 Garnesson, P., Mangin, A., Fanton d'Andon, O., Demaria, J., and Bretagnon, M.: The CMEMS GlobColour
460 chlorophyll a product based on satellite observation: multi-sensor merging and flagging strategies, *Ocean Sci.*,
461 15(3), 819-830, doi:10.5194/os-15-819-2019, 2019.

462 Good, S., Fiedler, E., Mao, C., Martin, M. J., Maycock, A., Reid, R., ... and Worsfold, M.: The current configuration
463 of the OSTIA system for operational production of foundation sea surface temperature and ice concentration
464 analyses, *Remote Sens-Basel.*, 12(4), 720, doi:10.3390/rs12040720, 2020.

465 Haarsma, R. J., Hazeleger, W., Severijns, C., de Vries, H., Sterl, A., Bintanja, R., ..., and van den Brink, H. W.:
466 More Hurricanes to Hit Western Europe Due to Global Warming, *Geophys. Res. Lett.*, 40, 1783–1788,
467 doi:10.1002/grl.50360, 2013.

468 Hart, R. E., and Evans, J. L.: A climatology of the extratropical transition of Atlantic tropical cyclones, *J. Climate*,
469 14(4), 546-564, doi:10.1175/1520-0442(2001)014<0546:ACOTET>2.0.CO;2, 2001.

470 Holton, J. R., and Hakim, G. J., *An Introduction to Dynamic Meteorology*, 5th ed., Vol. 88. San Diego, CA:
471 Academic Press, Elsevier, doi:10.1119/1.1987371, 2012.

472 Kawai, Y., and Wada, A.: Detection of cyclone-induced rapid increases in chlorophyll-a with sea surface cooling in
473 the northwestern Pacific Ocean from a MODIS/SeaWiFS merged satellite chlorophyll product, *Int. J. Remote Sens.*,
474 32(24), 9455-9471, doi:10.1080/01431161.2011.562252, 2011.

475 Knaff, J. A., Longmore, S. P., and Molenaar, D. A.: An objective satellite-based tropical cyclone size climatology, *J.*
476 *Climate*, 27(1), 455-476, doi:10.1175/JCLI-D-13-00096.1, 2014.

477 Knapp, K. R., Kruk, M. C., Levinson, D. H., Diamond, H. J., and Neumann, C. J.: The International Best Track
478 Archive for Climate Stewardship (IBTrACS), *B. Am. Meteorol. Soc.*, 91 (3), 363–376,
479 doi:10.1175/2009BAMS2755.1, 2010.

480 Kossin, J. P., Knapp, K. R., Olander, T. L., and Velden, C. S.: Global Increase in Major Tropical Cyclone
481 Exceedance Probability over the Past Four Decades, *P. Natl. A. Sci USA*, 117 (22), 11975–11980,
482 doi:10.1073/pnas.1920849117, 2020.

483 Krasnopolsky, V., Nadiga, S., Mehra, A., Bayler, E., and Behringer, D.: Neural networks technique for filling gaps
484 in satellite measurements: Application to ocean color observations, *Comput. Intel. Neurosc.*, 2016, 29,
485 doi:10.1155/2016/6156513, 2016.

486 Lavergne, T., Sørensen, A. M., Kern, S., Tonboe, R., Notz, D., Aaboe, S., ... and Pedersen, L. T.: Version 2 of the
487 EUMETSAT OSI SAF and ESA CCI sea-ice concentration climate data records, *The Cryosphere*, 13(1), 49-78,
488 doi:10.5194/tc-13-49-2019, 2019.

489 Lima, M. M. , Hurduc, A., Ramos, A. M. and Trigo, R. M.: The Increasing Frequency of Tropical Cyclones in the
490 Northeastern Atlantic Sector, *Front. Earth Sci.*, 9:745115, doi: 10.3389/feart.2021.745115, 2021.

491 Liu, X., Wang, M., and Shi, W.: A study of a Hurricane Katrina–induced phytoplankton bloom using satellite
492 observations and model simulations, *J. Geophys. Res-Oceans*, 114(C3), doi:10.1029/2008JC004934, 2009.

493 Maneesha, K., Murty, V. S. N., Ravichandran, M., Lee, T., Yu, W., and McPhaden, M. J.: Upper ocean variability in
494 the Bay of Bengal during the tropical cyclones Nargis and Laila, *Prog. Oceanogr.*, 106, 49-61,
495 doi:10.1016/j.pocean.2012.06.006, 2012.

496 Merchant, C. J., Le Borgne, P., Roquet, H., and Legendre, G.: Extended optimal estimation techniques for sea
497 surface temperature from the Spinning Enhanced Visible and Infra-Red Imager (SEVIRI), *Proc. SPIE*, 131, 287-297,
498 doi:10.1016/j.rse.2012.12.019, 2013.

499 Pan, J., Huang, L., Devlin, A. T., and Lin, H.: Quantification of typhoon-induced phytoplankton blooms using
500 satellite multi-sensor data. *Remote Sens-Basel*, 10(2), 318, doi:10.3390/rs10020318, 2018.

501 Pearce, R. P.: The physics of hurricanes. *Phys. Technol.*, 18(5), 215, 1987.

502 Price, J. F.: Upper ocean response to a hurricane. *J. Phys. Oceanogr.*, 11(2), 153-175, doi:10.1175/1520-
503 0485(1981)011<0153:UORTAH>2.0.CO;2, 1981.

504 Price, J. F., Sanford, T. B., and Forristall, G. Z.: Forced stage response to a moving hurricane. *J. Phys. Oceanogr.*,
505 24(2), 233-260, doi:10.1175/1520-0485(1994)024<0233:FSRTAM>2.0.CO;2, 1994.

506 Ramsay, H.: *The Global Climatology of Tropical Cyclones*. Oxford Research Encyclopedia of Natural Hazard
507 Science. Victoria, Australia: Oxford University Press, doi:10.1093/acrefore/9780199389407.013.79, 2017.

508 Saha, K., Zhao, X., Zhang, H., Casey, K. S., Zhang, D., Baker-Yeboah, S., ... and Relph, J. M.: AVHRR Pathfinder
509 version 5.3 level 3 collated (L3C) global 4km sea surface temperature for 1981-Present, NOAA National Centers for
510 Environmental Information, dataset, doi:10.7289/v52j68xx, 2018.

511 Sathyendranath, S., Brewin, R. J. W., Brockmann, C., Brotas, V., Calton, B., Chuprin, A., ... and Platt, T.: An
512 ocean-colour time series for use in climate studies: the experience of the Ocean-Colour Climate Change Initiative
513 (OC-CCI), *AH S. Sens.*, 19(19), 4285, doi:10.3390/s19194285, 2019.

514 Sathyendranath, S., Jackson, T., Brockmann, C., Brotas, V.; Calton, B., Chuprin, A., ... and Platt, T.: ESA Ocean
515 Colour Climate Change Initiative (Ocean_Colour_cci): Version 5.0 Data, NERC EDS Centre for Environmental
516 Data Analysis, 19 May 2021, doi:10.5285/1d8e7a109c0244aaad713e078fd3059a, 2021.

517 Saulquin, B., Gohin, F., and Fanton d'Andon, O.: Interpolated fields of satellite-derived multi-algorithm
518 chlorophyll-a estimates at global and European scales in the frame of the European Copernicus-Marine Environment
519 Monitoring Service. *J. of Oper. Oceanogr.*, 12(1), 47-57, doi:10.1080/1755876X.2018.1552358, 2019.

520 Shropshire, T., Li, Y., and He, R.: Storm impact on sea surface temperature and chlorophyll a in the Gulf of Mexico
521 and Sargasso Sea based on daily cloud-free satellite data reconstructions, *Geophys. Res. Letters*, 43(23), 12-199,
522 doi:10.1002/2016GL071178, 2016.

523 Subrahmanyam, B., Rao, K. H., Srinivasa Rao, N., Murty, V. S. N., and Sharp, R. J.: Influence of a tropical cyclone
524 on chlorophyll-a concentration in the Arabian Sea, *Geophys. Res. Letters*, 29(22), 22-1,
525 doi:10.1029/2002GL015892, 2002.

526 Taylor, H. T., Ward, B., Willis, M., and Zaleski, W.: *The saffir-simpson hurricane wind scale*. Atmospheric
527 Administration: Washington, DC, USA., 2010.

528 Walker, N. D., Leben, R. R., and Balasubramanian, S.: Hurricane-forced upwelling and chlorophyll-a enhancement
529 within cold-core cyclones in the Gulf of Mexico, *Geophys. Res. Letters*, 32(18), doi:10.1029/2005GL023716, 2005.

- 530 Zhang, J., Lin, Y., Chavas, D. R., and Mei, W.: Tropical cyclone cold wake size and its applications to power
531 dissipation and ocean heat uptake estimates. *Geophys. Res. Letters*, 46(16), 10177-10185,
532 doi:10.1029/2019GL083783, 2019.
- 533 Zheng, Z. W., Ho, C. R., and Kuo, N. J.: Importance of pre-existing oceanic conditions to upper ocean response
534 induced by Super Typhoon Hai-Tang. *Geophys. Res. Letters*, 35(20), doi:10.1029/2008GL035524, 2008.